Interpretation of Channeled-Ion Energy-Loss Spectra*

MARK T. ROBINSON
Solid State Division, Oak Ridge National Laboratory, Oak Ridge, Tennessee 37830
(Received 23 October 1968)

The energy-loss spectra produced in beams of energetic He and I ions transmitted through planar channels in thin Au monocrystals have been explained by a simple model in which the ions execute transverse anharmonic oscillations in the channel between a pair of adjacent planes of target atoms and in which the stopping power of the medium is a function of the distance of the ion from the crystal planes. A quantitative comparison of this model with recent experiments is made using a plane-averaged potential based on Moliere's approximation to the Thomas-Fermi screening function to describe the oscillatory motion. The stopping power is found to obey the same functional dependence on the coordinates, but with a doubled screening length. The parameters of the model may be deduced directly from the experimental data. For He in Au, these parameters agree well with those expected from Firsov's treatment of the interaction potential between neutral atoms. For I in Au, the high charge of the ion leads to parameters which differ significantly from Firsov's theory. The data also suggest that the energy dependence of the stopping power for channeled ions may be somewhat different from that for randomly directed ones.

I. INTRODUCTION

THE energy-loss spectra produced in beams of energetic He and I ions transmitted through thin gold monocrystals in directions lying very nearly in low index crystallographic planes have been reported recently.[1–3] These spectra consist of several well-resolved groups of particles, the number, spacing, and populations of which depend upon the particle energy, the crystal thickness, and the geometrical relationships among the incident beam, the crystallographic plane, and the narrow aperture detector. A qualitative account of many aspects of these spectra can be given by a simple model[1,2,4] in which the ions execute transverse anharmonic oscillations in the channel between a pair of adjacent planes of target atoms and in which the stopping power of the medium is a function of the displacement of the ion from the crystal planes. The objective of the present investigation is to make a quantitative comparison of this model with experiments reported by Datz *et al.*,[1] in an accompanying paper. It is necessary to select an interatomic potential and a stopping power function to solve the dynamical problem in a suitable approximation, to deduce model parameters appropriate to the experimental data, and to compare the predictions of the model with the observations. Throughout the investigation, classical mechanics was employed: the justifications for this procedure have been discussed recently by Datz *et al.*,[4] by Cowley,[5] and by Chadderton.[6]

The dynamical problem involves the slowing down of the incident ions through inelastic encounters with the atoms of the medium. This problem is first approximated by dividing the interaction of the ions with the medium into an elastic (conservative) part described by a static potential and an inelastic part described by a stopping power. No explicit correlation between the two functions will be considered beyond that implied by the form adopted for the spatial dependence of each. The experiments deal with incident ions of high energy, ~3 MeV for He and ~60 MeV for I, constrained to travel within ~0.5° of low index crystallographic planes. Because of their high speed, the ions move past individual target atoms in very nearly straight lines and their deflection is accomplished by interaction with a large number of lattice atoms. Thus, as long as incidence parallel to principal crystallographic axes is avoided, the atomic nature and detailed structure of the atomic planes may be ignored and the ions regarded as interacting with the planar potential

$$V_1(\bar{x}) = 4\pi\rho l \int_{\bar{x}}^{\infty} rU(r)dr, \qquad (1)$$

where $U(r)$ is the interaction potential between an ion and an atom separated by a distance r, ρ is the density of atoms in the medium, $\bar{x}$ is the length of the normal from the ion to the plane of lattice atoms, and l is one-half the spacing between the crystallographic planes. The dynamical problem is to consider, with suitable allowance made for the stopping power of the medium, the motion of the incident ion in the channel between two adjacent planes of lattice atoms, that is, in the potential

$$V(x) = V_1(l-x) + V_1(l+x), \quad -l < x < l \qquad (2)$$

where the origin is taken half-way between the two planes of atoms, a distance l from each. The planar potentials (1) and (2) should give a satisfactory description of the transverse motion of the ions as they pass through the crystal channel as long as their transverse kinetic energies are small enough, that is, as

* Research sponsored by the U. S. Atomic Energy Commission under contract with Union Carbide Corporation.
[1] S. Datz, C. D. Moak, T. S. Noggle, B. R. Appleton, and H. O. Lutz, preceding paper, Phys. Rev. 179, 315 (1969).
[2] H. O. Lutz, S. Datz, C. D. Moak, and T. S. Noggle, Phys. Rev. Letters 17, 285 (1966).
[3] W. M. Gibson, J. B. Rasmussen, P. Ambrosius-Olesen, and C. J. Andreen, Can. J. Phys. 46, 551 (1968).
[4] S. Datz, C. Erginsoy, G. Leibfried, and H. O. Lutz, Ann. Rev. Nucl. Sci. 17, 129 (1967).
[5] J. M. Cowley, Phys. Letters 26A, 623 (1968).
[6] L. T. Chadderton, Phil. Mag. 18, 1017 (1968).

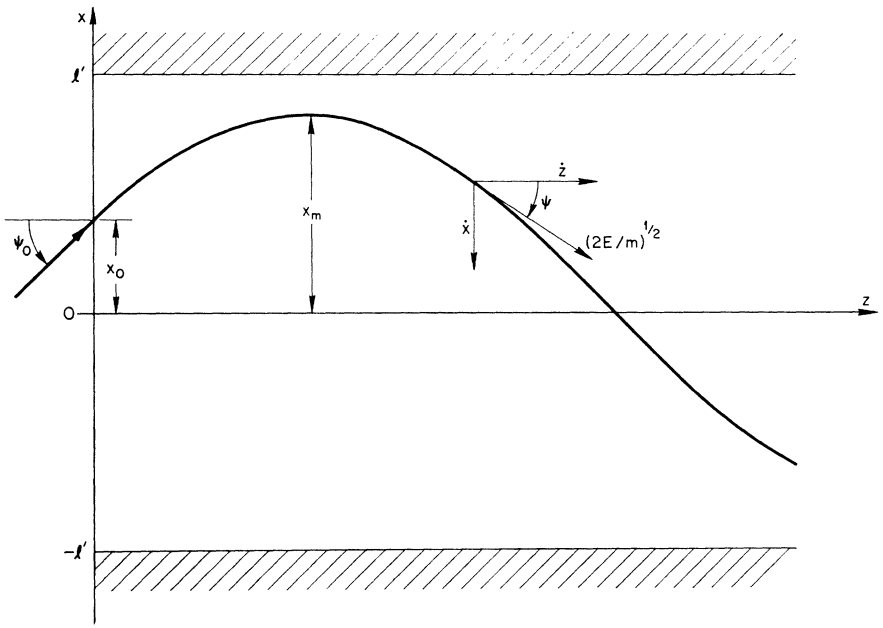

FIG. 1. The coordinates used in the dynamical problem.

long as

$$(\tfrac{1}{2}m\dot{x}^2)_{x=0} < V(l) - V(0). \tag{3}$$

Particles of greater transverse energy than this are likely to approach the lattice atoms very closely and are correspondingly likely to be scattered out of the channel.

The equations of motion to be solved are

$$m\ddot{x} + dV(x)/dx + S(x,E)\sin\psi = 0, \tag{4}$$

$$m\ddot{z} + S(x,E)\cos\psi = 0, \tag{5}$$

where $S(x,E)$ is the stopping power of the medium, $\psi(t)$ is the angle between the direction of motion of the ion and the channel plane, and $E(t) = \frac{1}{2}m(\dot{x}^2+\dot{z}^2)$ is the kinetic energy of the ion. The initial conditions are

$$x(t=0) = x_0, \quad \dot{x}(t=0) = (2E_0/m)^{1/2}\sin\psi_0, \tag{6}$$

$$z(t=0) = 0, \quad \dot{z}(t=0) = (2E_0/m)^{1/2}\cos\psi_0, \tag{7}$$

where m is the mass of the ion, x_0 is the impact parameter, E_0 is the incident kinetic energy of the ion, and ψ_0 is the angle of incidence of the beam. The coordinates used in discussing this problem are sketched in Fig. 1. Equations (4) and (5) may be rewritten

$$d[\tfrac{1}{2}m\dot{x}^2 + V(x)]/dx = -S(x,E)\sin\psi, \tag{8}$$

$$d[\tfrac{1}{2}m\dot{z}^2]/dz = -S(x,E)\cos\psi. \tag{9}$$

Because the direction of motion of the ion always remains within $\sim 0.5°$ of the channel plane, it is permissible to set $\cos\psi = 1$ and to identify the kinetic energy E with its longitudinal component $E\cos^2\psi = \frac{1}{2}m\dot{z}^2$, an approximation which will be used freely hereafter. At the same time, because $\sin\psi$ is small, it is a reasonable approximation to neglect the inelastic term in Eq. (8) and to describe the transverse oscillatory motion of the ion by the solution of the remaining conservative differential equation

$$\dot{x} = (2/m)^{1/2}[V(x_m) - V(x)]^{1/2}, \tag{10}$$

where x_m is the amplitude of the oscillatory motion defined by

$$V(x_m) = E_0\sin^2\psi_0 + V(x_0) < V(l). \tag{11}$$

Note that the critical channeling angle may be deduced from Eq. (11) by setting $x_m = l$, $x_0 = 0$, and solving for $\psi_0 = \psi_c$. Ions of incident angle $\psi_0 > \psi_c$ will not be channeled, but will break through the crystal planes and enter the unaligned beam.

After selecting a suitable interaction potential, Eq. (10) will be solved and the result used to discuss the geometrical aspects of the energy-loss spectra. Then a stopping-power function will be chosen so that Eq. (9) can be integrated. It will then be possible to make a quantitative comparison of the model with recent experiments[1] and to assess the errors introduced by neglecting the inelastic part of Eq. (8).

II. INTERATOMIC POTENTIAL

Erginsoy,[7] Lindhard *et al.*,[8] and Wedepohl[9] have recently discussed the choice of an interatomic potential function for use in calculations of atomic scattering. At small separations of two atoms, it is appropriate to use a screened Coulomb potential with a screening function

[7] C. Erginsoy, in *Interaction of Radiation with Solids*, edited by A. Bishay (Plenum Press, Inc., New York, 1967), p. 341; Phys. Rev. Letters **15**, 360 (1965).

[8] J. Lindhard, V. Nielson, and M. Scharff, Kgl. Danske Videnskab. Selskab, Mat.-Fys. Medd. **36**, No. 10 (1968).

[9] P. T. Wedepohl, Solid State Commun. **4**, 479 (1966); Proc. Phys. Soc. (London) **92**, 79 (1967); J. Phys. **B1**, 307 (1968).

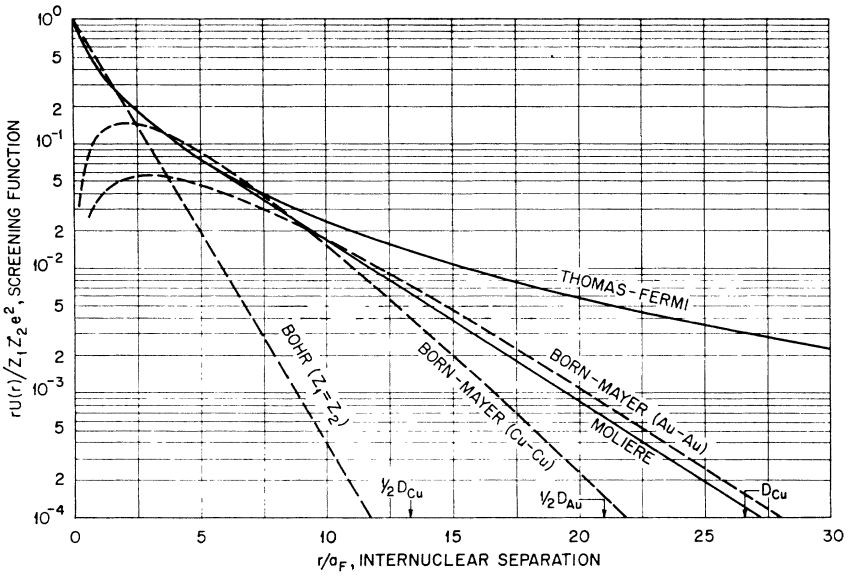

FIG. 2. Comparison of some interatomic potentials. The screening functions $rU(r)/Z_1Z_2e^2$ are plotted as functions of the internuclear separation in units of the Firsov screening length a_F. D indicates the nearest-neighbor distances in the crystals.

derived from Thomas-Fermi theory, in particular, as applied to atomic interactions by Firsov.[10] Although this potential decreases too slowly for large separations, the difficulty may be remedied in part by using the approximation to the Thomas-Fermi screening function[11] proposed by Moliere.[12] With this screening function, the interaction potential is

$$U(r)=(Z_1Z_2e^2/r)[0.35\exp(-br)+0.55\exp(-4br)+0.10\exp(-20br)], \quad (12)$$

where

$$b=0.3/a, \quad (13)$$

Z_1e and Z_2e are the nuclear charges of the two atoms, and a is a screening length, given, for example, by the proposal of Firsov[10]:

$$a_F=(9\pi^2/128)^{1/3}a_H(Z_1^{1/2}+Z_2^{1/2})^{-2/3}, \quad (14)$$

where $a_H=\hbar^2/me^2$ is the radius of the first Bohr orbit of hydrogen. A potential very similar to Moliere's has been proposed also by Csavinsky.[13] As shown in Fig. 2, the potential (12) falls off more rapidly than does that using the exact Thomas-Fermi screening function, and even gives reasonable agreement with empirical Born-Mayer potentials proposed to describe Cu-Cu [14] and Au-Au [15] interactions at separations near the normal lattice distance. The applicability of such potentials, based as they are on theories concerning the interaction of neutral atoms, to the interaction of highly charged ions with neutral atoms is, of course, doubtful. Nevertheless, one may hope to obtain some agreement between calculation and experiment by adjustment of the model parameters. The values of these parameters may then be a guide in improving the underlying theory. Combining Eqs. (12), (1), and (2), the planar potentials are

$$V_1(\bar{x})=(4\pi\rho Z_1Z_2e^2l/b)[0.35\exp(-b\bar{x})+0.1375\exp(-4b\bar{x})+0.005\exp(-20b\bar{x})] \quad (15)$$

and

$$V(x)=V_0[\cosh bx+(11/28)\cosh 4bx+(1/70)\cosh 20bx], \quad (16)$$

where

$$V_0=0.35(8\pi\rho Z_1Z_2e^2l/b)\exp(-bl). \quad (17)$$

Equations (15) and (16) are rather well approximated by their first terms, except close to the atomic planes, where the other terms become significant. The single-term approximation is even better when account is taken of the thermal motion of the lattice atoms, as has been described by Erginsoy.[7] The displacements of the atoms normal to the plane are assumed to be independent of each other and to be distributed according to a Gaussian. Then, each term $\exp(-nb\bar{x})$, $n=1$, 4, or 20, in Eq. (15) is replaced by a term

$$\tfrac{1}{2}\exp(n^2\gamma^2+nb\bar{x})\operatorname{erfc}(n\gamma+b\bar{x}/2\gamma)+\tfrac{1}{2}\exp(n^2\gamma^2-nb\bar{x})\operatorname{erfc}(n\gamma-b\bar{x}/2\gamma), \quad (18)$$

where

$$\gamma^2=\tfrac{1}{2}b^2\langle\Delta x^2\rangle, \quad (19)$$

and $\langle\Delta x^2\rangle$ is the mean-square displacement normal to the

[10] O. B. Firsov, Zh. Eksperim. i Teor. Fiz. **32**, 1464 (1957); **33**, 696 (1957); **34**, 447 (1958) [English transls.: Soviet Phys.—JETP **5**, 1192 (1957); **6**, 534 (1958); **7**, 308 (1958)].

[11] P. Gombas, in *Handbuch der Physik*, edited by S. Flügge (Springer-Verlag, Berlin, 1956), Vol. 36, p. 109.

[12] G. Moliere, Z. Naturforsch. **2a**, 133 (1947).

[13] P. Csavinsky, Phys. Rev. **166**, 53 (1968).

[14] J. B. Gibson, A. N. Goland, M. Milgram, and G. H. Vineyard, Phys. Rev. **120**, 1229 (1960).

[15] M. W. Thompson and R. S. Nelson, in Symposium on Atomic Collision Cascades in Radiation Damage, United Kingdom Atomic Energy Authority Report No. AERE-R4694, 1964 (unpublished); M. W. Thompson, Phil. Mag. **18**, 377 (1968).

plane. In Fig. 3, the functions $V_1(\bar{x},\gamma)$ are plotted for $\gamma=0$, 0.3, and 0.6, the first corresponding to Eq. (15) and the second being appropriate for Au near room temperature. As long as the asymptotic form of the first term of $V_1(\bar{x},\gamma)$ is less than $V_1(0,\gamma)$, it provides a convenient and satisfactory approximation to the complete function, as is shown by the dashed lines of Fig. 3. Thus, finally, the planar channel potential adopted is

$$V(x)=V_0'\cosh bx, \quad -l'\leq x\leq l' \tag{20}$$

where

$$V_0'=0.35(8\pi\rho Z_1Z_2e^2l/b)\exp(\gamma^2-bl)=V_0e^{\gamma^2}, \tag{21}$$

and b is defined by Eq. (13). The "effective" channel half-width is defined by

$$\begin{aligned} l'&=l, \quad 0\leq\gamma\leq 0.178999\\ &=l+(1/b)\ln[\operatorname{erfc}\gamma+(11/28)\exp(15\gamma^2)\operatorname{erfc}4\gamma\\ &\qquad +(1/70)\exp(399\gamma^2)\operatorname{erfc}20\gamma],\\ &\qquad 0.178999\leq\gamma\leq\infty. \end{aligned} \tag{22}$$

The limiting value of γ in Eq. (22) is that for which the extrapolated asymptotic form of the first term of $V_1(\bar{x},\gamma)$ passes through $V_1(0,\gamma)$. The effect of thermal vibrations is to narrow the channel somewhat and to lower the transverse kinetic energy necessary for escape from the channel, that is, to reduce the critical angle ψ_c. Neither effect is large, however, and, in view of the approximate nature of the present analysis, it will be justified to ignore thermal effects altogether. In the equations below, the thermally altered quantities V_0' and l' will be indicated; the primes are to be omitted when thermal effects are to be ignored.

III. OSCILLATORY MOTION

Using Eq. (20) for the interatomic potential, the differential equation (10) becomes

$$\dot{x}=(2V_0'/m)^{1/2}(\cosh bx_m-\cosh bx)^{1/2}. \tag{23}$$

Introducing the abbreviations

$$\begin{aligned} \eta&=[V(x_m)-V(0)]/[V(x_m)+V(0)]\\ &=(\cosh bx_m-1)/(\cosh bx_m+1)=\tanh^2\tfrac{1}{2}bx_m, \end{aligned} \tag{24}$$

$$\xi=b(V_0'/m)^{1/2}t, \tag{25}$$

$$\vartheta=(E/V_0')^{1/2}\sin\psi, \tag{26}$$

$$\vartheta_m=[2\eta/(1-\eta)]^{1/2}, \tag{27}$$

$$u=\xi(1-\eta)^{-1/2}, \tag{28}$$

the required solution of Eq. (23) may be written as

$$\vartheta=\vartheta_m\,\mathrm{sn}[\mathrm{sn}^{-1}(\vartheta_0/\vartheta_m|\eta)\pm u|\eta] \tag{29}$$

$$=\frac{\vartheta_m[\vartheta_0\vartheta_m\,\mathrm{cn}(u|\eta)\,\mathrm{dn}(u|\eta)\pm(\vartheta_m^2-\vartheta_0^2)^{1/2}(\vartheta_m^2-\eta\vartheta_0^2)^{1/2}\,\mathrm{sn}(u|\eta)]}{[\vartheta_m^2-\eta\vartheta_0^2\,\mathrm{sn}^2(u|\eta)]}, \tag{30}$$

where $\mathrm{sn}(u|\eta)$, $\mathrm{cn}(u|\eta)$, and $\mathrm{dn}(u|\eta)$ are three copolar Jacobian elliptic functions[16] of *argument* u and *parameter* η. The two signs in Eqs. (29) and (30) correspond to two closely related trajectories with the same amplitude, having $x(t=0)=\pm x_0$. Equation (30) is obtained from Eq. (29) by application of the addition formulas for the elliptic functions.[16]

The function ϑ is periodic in ξ with the period

$$\tau(\eta)=4(1-\eta)^{1/2}K(\eta), \tag{31}$$

where $K(\eta)$ is the complete elliptic integral of the first kind.[16] As η increases from 0 to 1, the period $\tau(\eta)$ decreases from 2π to 0, although for any particular channel there is a limiting value $\tau(\eta_{\max})$, where $\eta_{\max}$ is given by Eq. (24) with $x_m=l'$. Equation (31) provides the relationship between the amplitude and the period of oscillation of the channeled ion which is required in the model. The dependence of ϑ upon η is illustrated in Fig. 4 for two values of ϑ_0 and a particular value of ξ. The envelope of its oscillations, shown in Fig. 4 as a dotted line, is ϑ_m, defined by Eq. (27). The function is defined as long as $\eta_{\min}\leq\eta\leq\eta_{\max}$, where

$$\eta_{\min}=\vartheta_0^2/(2+\vartheta_0^2), \tag{32}$$

$$\vartheta(\eta_{\min})=\vartheta_0\,\mathrm{cd}(u|\eta_{\min}), \tag{33}$$

and where the elliptic function $\mathrm{cd}(u|\eta)=\mathrm{cn}(u|\eta)/\mathrm{dn}(u|\eta)$.[16] It should be noted that $\vartheta(\eta_{\min})$ may have any value between $-\vartheta_0$ and ϑ_0, depending on the value of ξ, and is only accidentally equal to ϑ_0. A property of ϑ that is important in discussing the geometrical aspects of the energy-loss spectra may be summarized by the nodal formulas

$\vartheta=\vartheta_0$, when

$$\xi=n\tau(\eta) \tag{34}$$

$$=(n+\tfrac{1}{2})\tau(\eta)\pm 2(1-\eta)^{1/2}\,\mathrm{sn}^{-1}(\vartheta_0/\vartheta_m|\eta); \tag{35}$$

$\vartheta=-\vartheta_0$, when

$$\xi=(n+\tfrac{1}{2})\tau(\eta) \tag{36}$$

$$=n\tau(\eta)\pm 2(1-\eta)^{1/2}\,\mathrm{sn}^{-1}(\vartheta_0/\vartheta_m|\eta); \tag{37}$$

[16] E. H. Neville, *Jacobian Elliptic Functions* (Oxford University Press, Oxford, 1951), 2nd ed.; P. F. Byrd and M. D. Friedman, *Handbook of Elliptic Integrals for Engineers and Physicists* (Springer-Verlag, Berlin, 1954); L. M. Milne-Thompson, in *Handbook of Mathematical Functions*, edited by M. Abramowitz and I. A. Stegun (U. S. Department of Commerce, National Bureau of Standards, Washington, 1965), Appl. Math. Ser. 55, p. 567. Note that in some of the above, the *modulus* $k=\eta^{1/2}$ is employed.

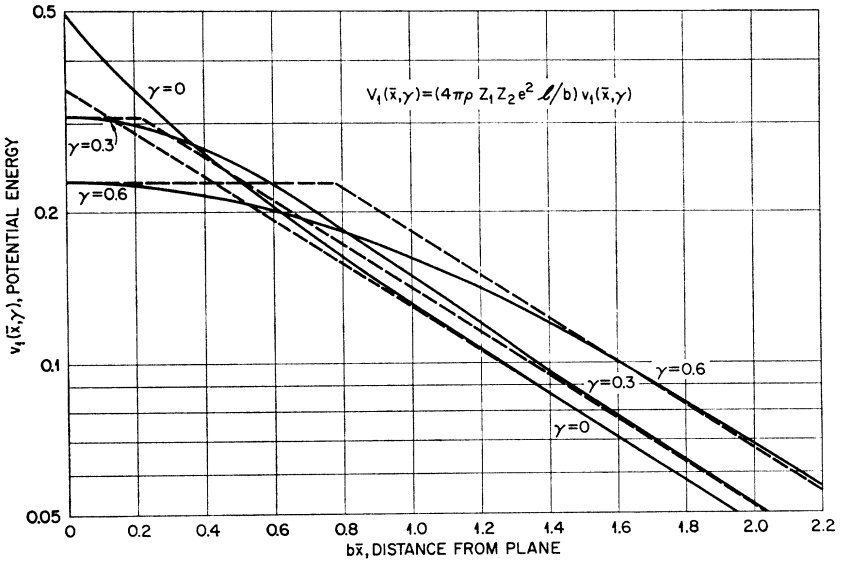

Effect of Thermal Vibrations on the Planar Moliere Potential.

FIG. 3. Effects of thermal vibrations on the planar Moliere potential. The function plotted is $v_1(\bar{x},\gamma)=(b/4\pi\rho Z_1 Z_2 e^2 \mathscr{l})\, V_1(\bar{x},\gamma)$. The solid lines show the full potential, the dashed lines the approximation discussed in the text.

here n is an integer. Note that when $\vartheta_0=0$, Eqs. (35) and (37) reduce to Eqs. (36) and (34), respectively.

IV. GEOMETRICAL ASPECTS OF ENERGY-LOSS SPECTRA

If the channeled ions moved through the crystal at a constant velocity, the variables ξ and ϑ, defined in Eqs. (25) and (26), could be interpreted as the pathlength through the crystal and the angle of emergence of the channeled ion from the crystal, respectively. Since the ion velocities decrease by less than $\sim 15\%$ in the experiments, this correlation is accurate enough for many applications. At the same time, however, since the energy lost by the ion is assumed to depend upon the amplitude of its oscillation, the variable η may be interpreted as a nonlinear analog of this energy loss: $\eta=0$ corresponds to the minimum energy loss of the most perfectly channeled ion. The dependence of the energy loss on the oscillation amplitude will be discussed below. This correlation of variables permits Fig. 4 to be interpreted as a plot of the angle with which ions emerge from the crystal (ϑ) against the energy which they lose (η), for a particular pathlength (ξ), and for two values of the angle of incidence (ϑ_0) of a beam of ions. In this approximation, it is useful to speak of the wavelength of a trajectory, that is, the product of the (constant) longitudinal velocity and the period of oscillation.

The solid curve of Fig. 4 corresponds to $\vartheta_0=0$. In this case, a detector collinear with the incident beam, that is, placed at $\vartheta=0$, will detect groups of particles

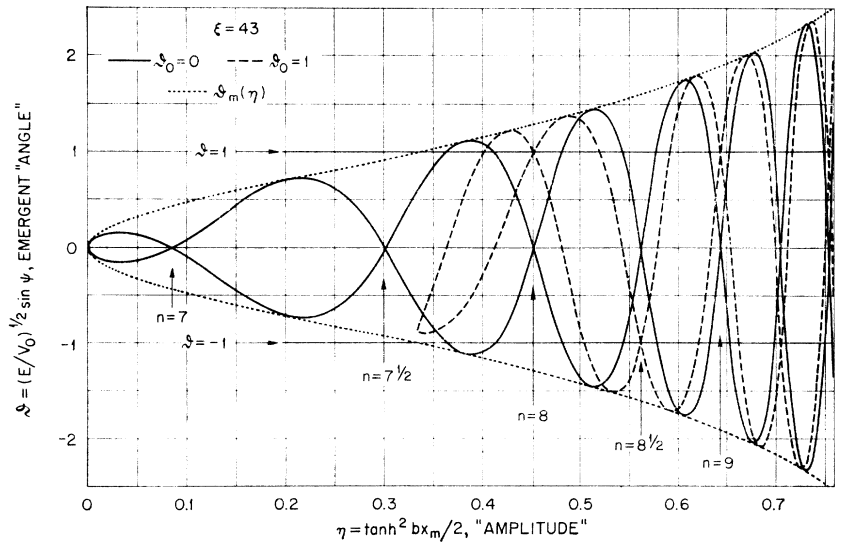

FIG. 4. The emergent "angle" ϑ as a function of the "amplitude" η for $\xi=43$ and $\vartheta_0=0$, 1. The dotted curve shows the values of $\vartheta_m(\eta)$, the angle with which a particle of amplitude η crosses the channel midplane.

only at $\eta=0$ and at the points marked $n=7$, $7\frac{1}{2}$, 8, etc. The first group is that termed A_0 in the experimental data; that is, the group of particles of very small oscillation amplitude. The other groups correspond to those particles making 7, $7\frac{1}{2}$, etc., oscillations in the channel as they pass through the crystal, that is, to the values given by the nodal equations (34) and (36). If the *detector* is moved away from $\vartheta=0$, the groups split, merge, and move in energy and emergent angle as the curves of Fig. 4 indicate. A similar interpretation applies when the beam (or crystal) is moved away from $\vartheta_0=0$. Here the important feature to note is that the *integer* nodes, Eq. (34), always occur at $\vartheta=\vartheta_0$; they will, therefore, always be present when the detector is collinear with the incident beam, whatever the angle of incidence. This is clearly shown by Eq. (34), which is independent of ϑ_0. In the same way, the *half-integer* nodes, Eq. (36), always occur at $\vartheta=-\vartheta_0$, that is, at what might be termed the "specular" angle. Equations (35) and (37) describe the phase-dependent groups, the locations of which are *not* independent of ϑ_0.

With these remarks in mind, it is possible to assess the effects of crystal misalignment and of ion beam divergence on the energy-loss spectra recorded with a detector which is collinear with the incident beam, this being the most frequently used experimental arrangement. A slightly misaligned region of the crystal, that is, a mosaic block regarded as running entirely through the target, results in the incident ions entering the channel at an angle deviating from the average, but the beam and detector are nevertheless still collinear. Hence the *integer* groups will still occur at the same values of η (i.e., energies) as in perfectly aligned regions. The half-integer and phase-dependent groups, however, will move to different values of η and ϑ. The solid and dashed curves of Fig. 4 illustrate this, the first, say, representing a perfectly aligned region, while the second represents a misaligned mosaic block. A detector collinear with the beam will record (at the same time) the $\vartheta=0$ line from the first and the $\vartheta=1$ line from the second. The coherence between the integer groups on the two lines means that they will appear as well-marked groups in the observed spectra, whereas the incoherent phase-dependent and half-integer groups will be spread over wide ranges of energy and emergent angle. Thus it may be asserted that the *integer* groups will persist even in crystals with large mosaic spread, at least as long as the blocks extend entirely through the sample. The half-integer and phase-dependent groups, however, will not persist as clear features in a collinear spectrum. The effects of beam divergence will destroy the integer groups as well. A divergent incident ray corresponds to a noncollinear detector. Hence, again referring to Fig. 4, the $\vartheta=0$ line of both solid and dashed curves would be recorded and no group coherence would be found. Thus experiments on energy-loss spectra must strive to lower beam divergence but need not be concerned particularly about crystal mosaic spread. In fact, as will be shown later, artificial exaggeration of mosaic spread by rocking the target crystal is a very useful technique.

If the crystal pathlength (i.e., ξ) is changed, the integer groups will move in a way described by Eq. (34). For a given value of n, as ξ increases, $\tau(\eta)$ must increase, or, as noted after Eq. (31), η decreases. Eventually, $\tau(\eta)$ reaches its limiting value 2π, and the group with this value of n is no longer possible. In fact, the limiting values of n that are possible at a given thickness are set by the inequalities

$$\xi/2\pi \leq n < \xi/\tau(\eta_{\max}). \tag{38}$$

The half-integer groups move in a precisely similar manner, as described by Eq. (36).

V. STOPPING POWER

In order to make a quantitative comparison of the predictions of the model with experiment, it is necessary to select a suitable stopping-power function $S(x,E)$ so that Eq. (9) may be integrated. Unfortunately, there is at present no very satisfactory theoretical or experimental basis on which to establish a form for this function. Guided by experimental data on the stopping power of polycrystalline media, it appears reasonable to separate the energy and coordinate dependence and to write

$$S(x,E)=s(x)E^p, \tag{39}$$

where the exponent p is to be chosen by reference to observation. The experimental data of Moak and Brown[17] on the stopping power of several polycrystalline targets for 20- to 120-MeV I ions are consistent with $p=\frac{1}{2}$, a value supported as well by theoretical investigations of low-energy electronic stopping.[18–20] For the 3-MeV He-ion experiments, p may be expected to be somewhat less than zero, since here the energy is slightly above that corresponding to the maximum stopping power. The experimental data[18] suggest $p\sim-\frac{1}{4}$ for 2- to 3-MeV He ions in Au. In both cases, p should decrease slowly with increasing energy, approaching -1 in the (nonrelativistic) high-energy limit.

The spatial factor $s(x)$ is more difficult to deal with. The ion slows down in part by resonant interactions with distant electrons and in part by collisions with electrons encountered along its path, the two contributions being of about equal size for randomly directed particles.[20] The former contribution is (presumably) independent of the coordinates of the decelerating ion, but the latter is expected to increase as the ion approaches the crystal planes, perhaps roughly paralleling

[17] C. D. Moak and M. D. Brown, Phys. Rev. Letters **11**, 284 (1963).
[18] L. C. Northcliffe, Ann. Rev. Nucl. Sci. **13**, 67 (1963).
[19] J. Lindhard and M. Scharff, Kgl. Danske Videnskab. Selskab, Mat.-Fys. Medd. **27**, No. 15 (1953).
[20] J. Lindhard and A. Winther, Kgl. Danske Videnskab. Selskab, Mat.-Fys. Medd. **34**, No. 4 (1964).

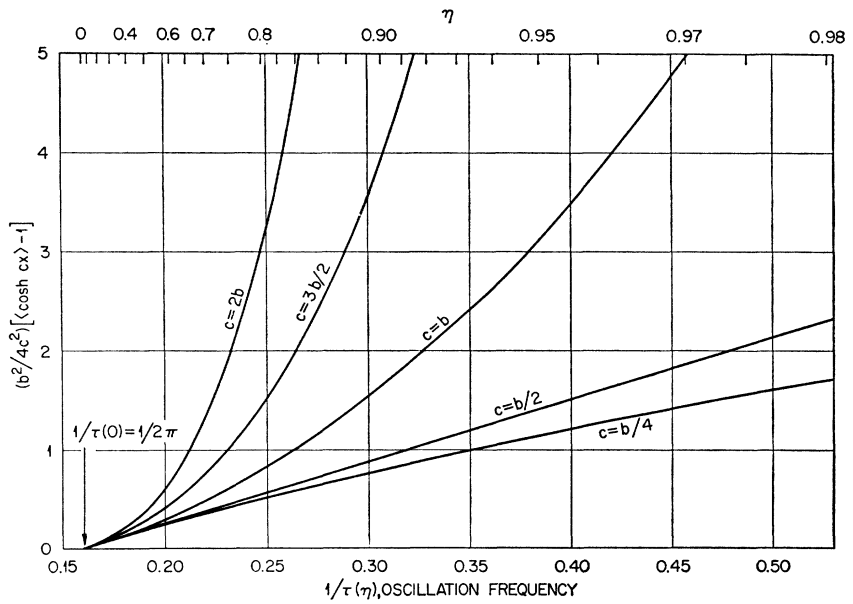

FIG. 5. The mean stopping power functions $\langle\cosh cx\rangle$ as functions of the oscillation frequency $1/\tau(\eta)$.

the corresponding increase in the density of electrons near the channel walls. In the case of the I ions, however, some part of the stopping presumably involves their own excitation and cannot be treated simply in terms of the electron density of the medium. In this rather unsatisfactory state of affairs, it has seemed appropriate to attempt to fit the available experimental data using arbitrary functions for $s(x)$ and to leave to future efforts the justification of the results.

Using Eq. (39) for the stopping power, Eq. (9) is readily integrated to give

$$E=[E_0^{1-p}-\langle s(x)\rangle(1-p)z]^{1/(1-p)}, \quad p\neq 1 \tag{40}$$

$$=E_0\exp[-\langle s(x)\rangle z], \quad p=1 \tag{41}$$

and

$$t=[(2m)^{1/2}/\langle s(x)\rangle(1-2p)](E_0^{1/2-p}-E^{1/2-p}), \quad p\neq\tfrac{1}{2} \tag{42}$$

$$=[(\tfrac{1}{2}m)^{1/2}/\langle s(x)\rangle]\ln(E_0/E), \quad p=\tfrac{1}{2} \tag{43}$$

where the initial conditions are derived from Eq. (7) and where $\langle s(x)\rangle$ is the value of $s(x)$ averaged over the transverse oscillatory motion of the channeled ion. If p is known, experimental observations of E as a function of the pathlength of the ions in the crystal can be used with Eqs. (40)–(43) to deduce empirical values of $\langle s(x)\rangle$ and of t for comparison with the model. More convenient empirical variables are the initial stopping power and the oscillation "frequency," defined according to

$$(-dE/dz)_{E=E_0}=\langle s(x)\rangle E_0^p, \tag{44}$$

$$\omega=n(2m)^{1/2}/t, \tag{45}$$

where n is the number of periods of the oscillatory motion executed by the ion in passing through the crystal. Most of the observations[1] refer to the case where the incident beam and the detector are collinear, so that n is integral or half-integral. As long as the number of quarter periods is integral, and approximately otherwise, the mean stopping power function in the model is given by

$$\langle s(x)\rangle=\left(\int_0^{x_m} s(x)\frac{dx}{\dot{x}}\right)\Big/\int_0^{x_m}\frac{dx}{\dot{x}}, \tag{46}$$

where $\dot{x}$ is given by Eq. (23). The integral in the denominator is simply the quarter period $\frac{1}{4}\tau$. The integral (46) may be evaluated easily for the functions $\cosh cx$, where c has such values as 0, $\frac{1}{4}b$, $\frac{1}{2}b$, etc. The results obtained are

$$\langle\cosh\tfrac{1}{4}bx\rangle=K(\tfrac{1}{2}[1-\{1-\eta\}^{1/2}])/(1-\eta)^{1/4}K(\eta), \tag{47}$$

$$\langle\cosh\tfrac{1}{2}bx\rangle=\pi/2(1-\eta)^{1/2}K(\eta)=2\pi/\tau(\eta), \tag{48}$$

$$\langle\cosh bx\rangle=2E(\eta)/(1-\eta)K(\eta)-1, \tag{49}$$

$$\langle\cosh\tfrac{3}{2}bx\rangle=[(1+\eta)/(1-\eta)]\langle\cosh\tfrac{1}{2}bx\rangle, \tag{50}$$

$$\langle\cosh 2bx\rangle=[4(1+\eta)/3(1-\eta)]\langle\cosh bx\rangle-\tfrac{1}{3}. \tag{51}$$

In Eq. (49), $E(\eta)$ is the complete elliptic integral of the second kind.[16] As indicated explicitly by the second form of Eq. (48), $\langle\cosh\frac{1}{2}bx\rangle$ is inversely proportional to the period of the oscillatory motion. That is, for this stopping-power function, the initial stopping power [Eq. (44)] would be directly proportional to the oscillation frequency ω [Eq. (45)]. The five functions, Eqs. (47)–(51), are plotted in Fig. 5 as functions of the oscillation frequency $1/\tau(\eta)$.

In order to select among the functions defined by Eqs. (47)–(51), use must be made of the experimental observations.[1] For each orientation of the gold target crystal, {100} and {111}, and for each ion, 3-MeV He and 60-MeV I, data were obtained on the positions of

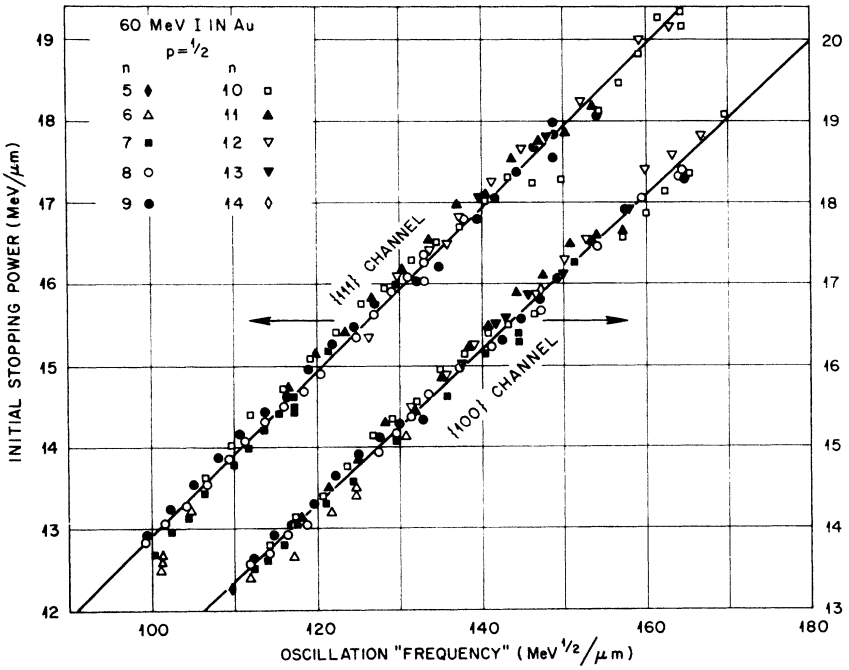

FIG. 6. The initial stopping power as a function of the oscillation frequency ω observed (Ref. 1) for 60-MeV I ions in Au {100} and {111} channels. The straight lines are least-squares fits to the observations. The energy exponent was assumed to be $p=\frac{1}{2}$.

the observed energy-loss groups as functions of the crystal pathlength, for the case of a detector collinear with the incident beam. Using Eqs. (40)–(45), plots were prepared of the initial stopping power as a function of the channel oscillation frequency. Initially, it was assumed that $p=\frac{1}{2}$ for the I ions and $p=0$ for the He ions. The integers n were chosen to give the best fit to the data. Half-integer groups were assumed to be absent from the observations. The results are shown in Fig. 6 for the I ions and in Fig. 7 for the He ions. Within the experimental uncertainties, each of the four sets of points is quite accurately represented by a straight line. Because of this very good fit, the form adopted for the spatial dependence of the model stopping power is

$$\langle s(x)\rangle = s_0 + s_1(\langle \cosh \tfrac{1}{2}bx\rangle - 1)\,, \qquad (52)$$

where s_0 represents the stopping power of the medium for ions moving exactly along the channel midplane, which may be determined from the observations, and s_1 is a constant also to be determined from the data. The slight curvature in the data of Figs. 6 and 7 is such that values of $c<\frac{1}{2}b$ cannot be rigorously excluded. However, the simplicity of Eq. (52) and the possi-

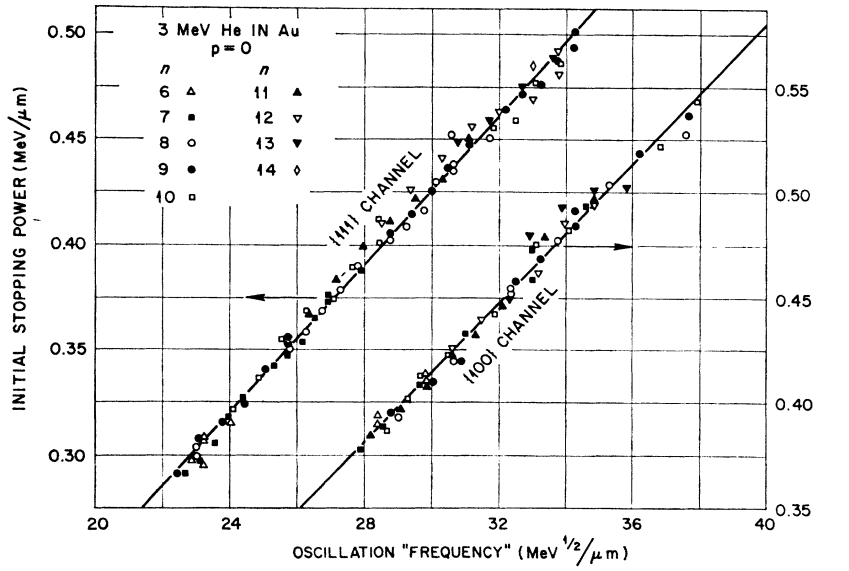

FIG. 7. The initial stopping power as a function of the oscillation frequency ω observed (Ref. 1) for 3-MeV He ions in Au {100} and {111} channels. The straight lines are least-squares fits to the observations. The energy exponent was assumed to be $p=0$.

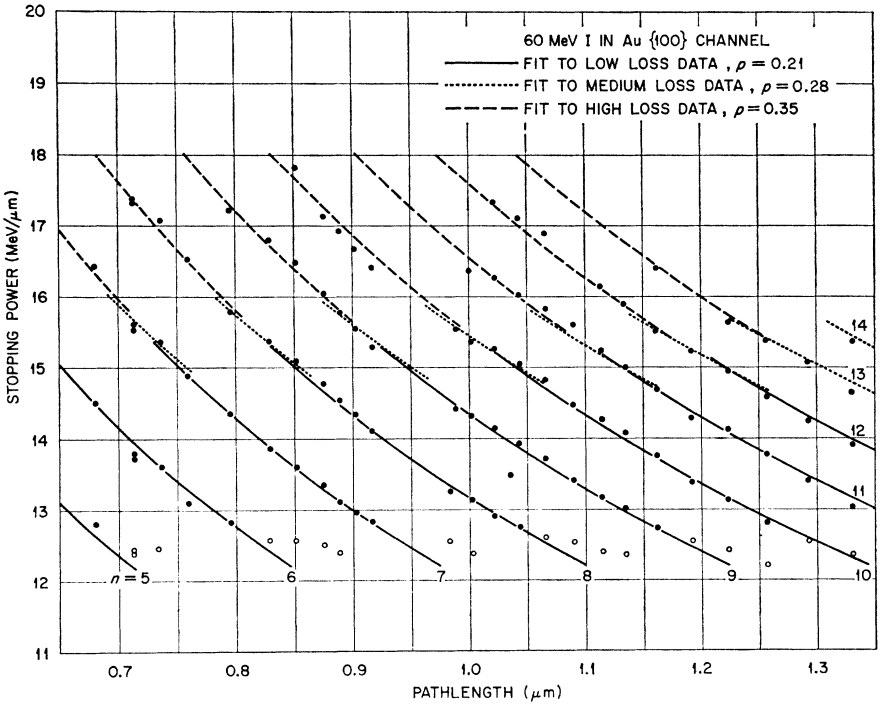

FIG. 8. Stopping power as a function of pathlength for 60-MeV I ions in the Au {100} channel. The points represent the experimental observations (Ref. 1); the curves are derived from the straight lines fitted to plots of initial stopping power against oscillation "frequency." The open circles were excluded from the fitting procedure. The parameters are shown in Table III.

bility that the curvature results from other factors are encouragements to proceed as outlined. Although its significance, if any, is presently unknown, it may be pointed out that the single-plane stopping power related to Eq. (52) is $\sim\exp(-\frac{1}{2}b\tilde{x})$, that is, to the square root of the single-plane potential $V_1(\tilde{x})$.

VI. DEDUCTION OF MODEL PARAMETERS FROM EXPERIMENTAL DATA

The complete model for describing the energy-loss spectra consists of the description of the oscillatory motion of the ions by Eqs. (29) or (30) and that of their slowing down by Eqs. (40)–(43), (48), and (52). The various model parameters may be deduced directly from the straight lines of Figs. 6 and 7, together with experimental observations of the minimum energy loss in each channel. The parameters of the straight line are easily related to the model parameters through Eqs. (25), (34), (44), and (52). The intercept is

$$\alpha=(s_0-s_1)E_0{}^p, \tag{53}$$

and the slope is

$$\beta=2^{1/2}\pi s_1E_0{}^p/bV_0{}^{1/2}. \tag{54}$$

From these parameters and the minimum stopping power $s_0E_0{}^p$, a value of $bV_0{}^{1/2}$ may be derived for each combination of ion and crystal plane. Inserting the two values of $bV_0{}^{1/2}$ for each ion into Eq. (17) [or (21)], a pair of equations is obtained which may be solved simultaneously for values of the potential parameter b and the product Z_1Z_2 (or $Z_1Z_2\exp\gamma^2$ if thermal effects are not ignored). The method of least squares was used to derive the values and standard deviations of α and β;

TABLE I. Model parameters derived from energy-loss spectra using *a priori* energy exponents.

	3-MeV He ions		60-MeV I ions	
	{100}	{111}	{100}	{111}
Channel half-width l, Å	1.0197	1.1774	1.0197	1.1774
Minimum stopping power, eV/Å	30.9±0.3	24.2±0.7	1280±20	1170±12
Intercept, eV/Å	−8.21±0.84	−10.2±0.5	302±13	280±13
Slope, $eV^{1/2}$	16.5±0.3	17.6±0.2	94.3±1.0	101±1
b^2V_0/l, $eV/Å^3$	108±6	64±3	2080±90	1290±50
b, $Å^{-1}$ (obs)	3.32±0.44		3.03±0.37	
$0.3/a_F$, $Å^{-1}$ (theor)	3.032		4.094	
Z_1Z_2 (obs)	129±46		2010±590	
Z_1Z_2 (theor)	158		4187	

TABLE II. Energy exponents derived from experimental data.

	3-MeV He ions {100}	3-MeV He ions {111}	60-MeV I ions {100}	60-MeV I ions {111}
A priori estimates	0	0	$\frac{1}{2}$	$\frac{1}{2}$
Minimum stopping power	0.02	−3.18	0.03	−0.14
All data	−0.14	−0.43	0.27	0.22
Low-loss data	0.14	−0.63	0.21	0.18
Medium-loss data	···	···	0.28	···
High-loss data	−0.22	−0.34	0.35	0.32

estimated standard deviations of other quantities were derived from these by conventional methods. The resulting analysis is displayed in Table I. A somewhat better fit to the data can be achieved by adjusting the energy exponent p. The "best" values of p are displayed in Table II for each ion-channel combination and for different schemes of grouping the data. The parameters derived from the low-loss data using the best values of p are displayed in Table III. As may be seen by comparison of Tables I and III, the values of the model parameters are little influenced by the choice of the energy exponent. The curves of stopping power as a function of crystal pathlength derived from the parameters of Table III are compared directly with the experimental observations in Fig. 8, for 60-MeV I ions in the Au {100} channel.

If each of the integers n assigned to the observed groups was increased or decreased by 1 and the fitting procedure was repeated, the best values of p were well outside the range $-1<p\leq\frac{1}{2}$, expected on theoretical grounds. This seems to support the chosen assignment of values.

The behavior of the energy exponents in Table II suggests that the stopping power of channeled ions may depend differently upon energy than it does for randomly directed ions. Unfortunately, of course, the results also suggest that p is a continuous function of the transverse coordinate or, what is the same thing, that the form adopted for the stopping power, Eq. (39), is not altogether appropriate. Since the results reported here are based on data obtained over only a rather small energy range, however, too much reliance should not be placed in them. Particular experiments to examine the energy dependence of the channeled-ion stopping power are planned.

The potential parameters derived from the He data are in reasonable agreement with those expected from Firsov's treatment of atomic interactions,[10] in spite of the inapplicability of the Thomas-Fermi approach to atoms as light as He. The parameters derived from the I data, however, are not in agreement with Firsov's work. The product Z_1Z_2 is about half that obtained from the nuclear charges, and the screening parameter b is significantly smaller than the Firsov value for neutral atoms. These differences are in the direction to be anticipated for interaction of the highly charged I atom with (nearly) neutral Au, but a consistent "effective" charge cannot be assigned to the two particles using Eq. (14). Allowance for thermal effects would leave the values deduced for b unaltered, but would lower the values obtained for Z_1Z_2 by the factor $\exp\gamma^2$, perhaps about 10%. This cannot be the explanation of the small values found for Z_1Z_2. It will be interesting to see how the potential parameters vary when deduced from experimental data obtained at significantly different incident ion energies.

The potential parameters of Table III may be used to establish a scale for the amplitude of oscillation of the channeled ions. A minimum and maximum distinguishable amplitude may be obtained for each combination of ion and channel from the extreme values observed for the oscillation frequencies. These extreme amplitudes are listed in Table IV, together with the fractions of the channel width associated with the leading group A_0 and with the region near the channel wall. In the case of the I ion, the derived maximum amplitudes are rather large, implying that the model potential rises a little too slowly near the channel walls. If potential parameters derived from the high-loss data are used, this situation is somewhat improved, however. It also appears from the fraction of the channel associated with the wall region in each case that He ions may be dechanneled more easily than I ions, a result

TABLE III. Model parameters derived from low energy-loss data using best-fit energy exponents.

	3-MeV He ions {100}	3-MeV He ions {111}	60-MeV I ions {100}	60-MeV I ions {111}
Minimum stopping power, eV/Å	29.5±0.1	21.1±0.3	1218±0.3	1090±3
Intercept, eV/Å	−8.5±1.1	−11.4±0.6	300±21	247±14
Slope, $eV^{1/2}$	16.8±0.4	17.5±0.2	90.0±1.7	98.6±1.2
b^2V_0/l, eV/Å^3	100±7	57±3	2010±126	1230±50
$b(V_0E_0)^{1/2}$, eV/Å	17 500	14 300	351 000	295 000
b, Å^{-1} (obs)	3.49±0.53		3.13±0.47	
$0.3/a_F$, Å^{-1} (theor)	3.032		4.094	
Z_1Z_2 (obs)	134±61		2100±800	
Z_1Z_2 (theor)	158		4187	

expected from their masses. The large fraction of the channel associated with the midplane region accounts for the great importance of the A_0 group.

The potential parameters of Table III may also be used to relate the model to the experimental results of Gibson *et al.*[3] on energy-loss spectra of 0.8-MeV He ions in very thin Au crystals. Using the parameters in the table and ignoring the slowing down of the channeled ions, the wavelengths of 0.8-MeV He ions in the Au {111} channel are predicted to range from 912 Å for zero amplitude to 434 Å at the maximum amplitude. In a pathlength of 1595 Å, corresponding to the data in Gibson's Figs. 9–12, from 1.7 to 3.3 oscillations could occur. Thus, it would be expected that the spectrum would consist of the A_0 group and the integer groups $n=2$ and 3, the former probably not resolvable from A_0. In a pathlength of 1396 Å, corresponding to Gibson's Fig. 13, from 1.5 to 2.9 oscillations could occur. Here, the $n=2$ group should be resolved from A_0, but $n=3$ should not appear. In either case, two groups ought to be observed, in general agreement with the experiments. The relatively poor resolution obtained in these spectra may result from the presence of fairly intense half-integer groups or, more likely, from the rather large values of detector acceptance angle and beam divergence used in these experiments. The changes in the spectra when the crystal is tilted support the latter interpretation.

TABLE IV. Oscillation amplitude scale derived from low energy-loss data.

	3-MeV He ions {111}	3-MeV He ions {100}	60-MeV I ions {111}	60-MeV I ions {100}
Channel half-width, Å	1.1774	1.0197	1.1774	1.0197
Minimum distinguishable amplitude, Å	0.53	0.55	0.51	0.34
Fraction of channel associated with leading group	0.45	0.54	0.43	0.33
Maximum distinguishable amplitude, Å	1.01	0.91	1.16	1.00
Fraction of channel associated with wall region	0.14	0.11	0.01	0.02

VII. ERROR DUE TO NEGLECT OF DAMPING

The transverse oscillatory motion of the channeled ion has been described by Eq. (8) with its inelastic term omitted. It is necessary to estimate the error introduced by this procedure. Using Eq. (39) for the stopping power, Eq. (8) may be rewritten

$$dV(x_m) = -(m/2)^{1/2}E^{p-1/2}\dot{x}s(x)dx\,, \tag{55}$$

where the total energy $V(x_m)$, defined by Eq. (11), is no longer constant. As long as the change in $V(x_m)$ is small, the transverse velocity may still be described by Eq. (10), and Eq. (55) may be integrated over a quarter period of the oscillatory motion. Introducing the definitions (24) and (31), the change in period occurring during one full oscillation period can be approximated by

$$\Delta\tau/\tau = (E^{p-1/2}/bV_0^{1/2})\sigma(\eta)\,, \tag{56}$$

where

$$\sigma(\eta) = \{(1-\eta)[1-E(\eta)/K(\eta)]/\eta\}b \times \int_0^{x_m} [\cosh bx_m - \cosh bx]^{1/2}s(x)dx. \tag{57}$$

The integral in Eq. (57) can be evaluated for $s(x)$

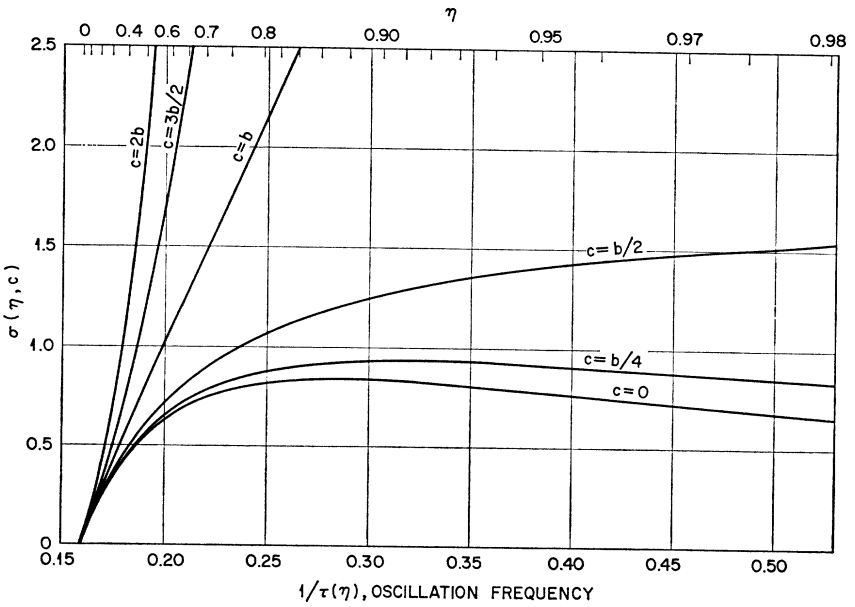

FIG. 9. The effect of damping on the transverse oscillation period, as a function of the oscillation frequency.

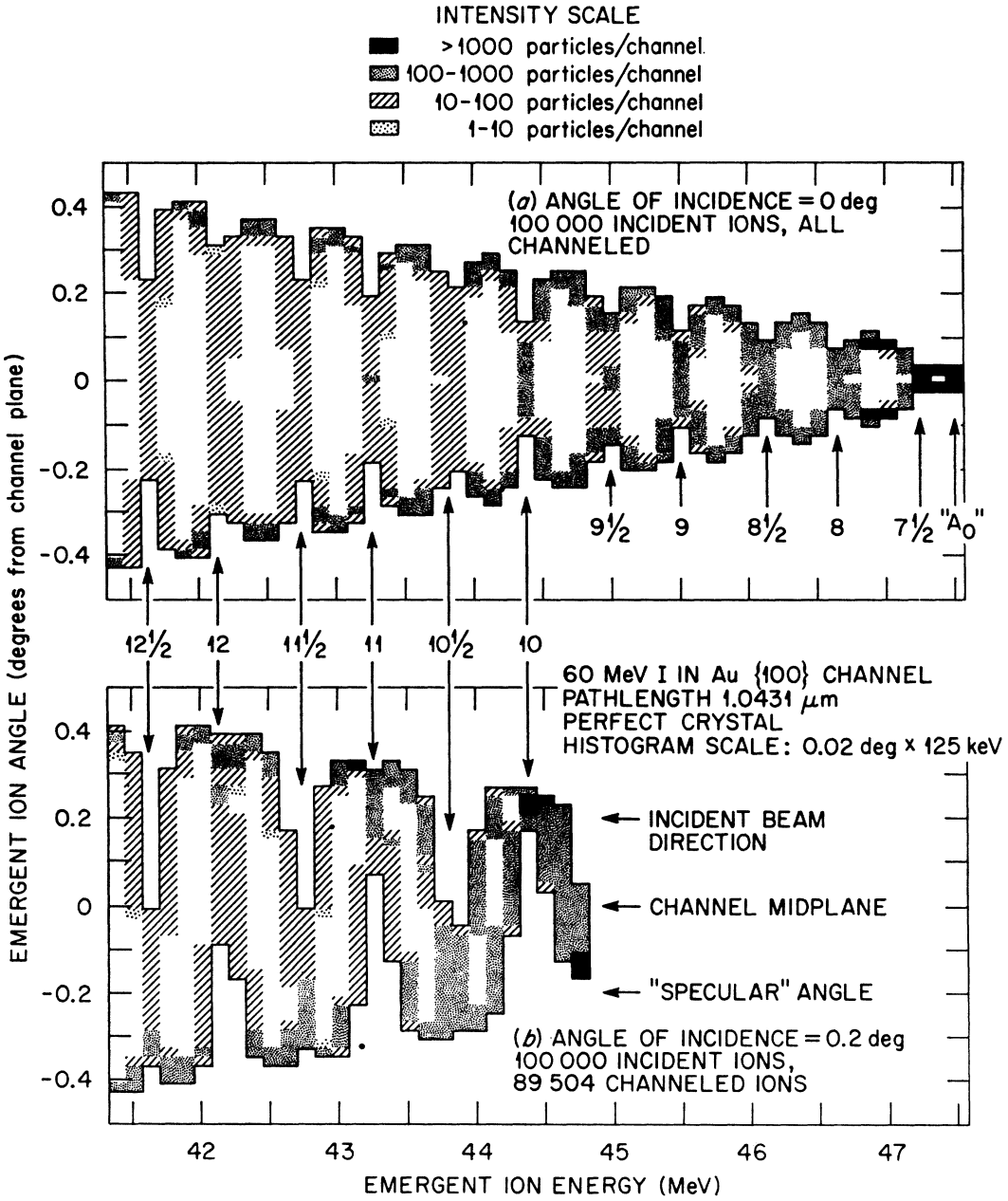

FIG. 10. Complete energy-loss spectra computed for 60-MeV I ions incident upon a perfect Au {100} channel, showing the effects of the incident angle. Model parameters are listed in Table III.

$\sim\cosh cx$, $c=0, \frac{1}{4}b, \frac{1}{2}b$, etc., as was done for the integrals of Eq. (46). The resulting functions $\sigma(\eta,c)$ include the following:

$$\sigma(\eta,0)=2^{3/2}(1-\eta)^{1/2}[K(\eta)-E(\eta)]^2/\eta K(\eta)\,, \tag{58}$$

$$\sigma(\eta,\tfrac{1}{4}b)=2^{5/2}(1-\eta)^{1/4}[K(\eta)-E(\eta)] \times([1+(1-\eta)^{1/2}]K\{\tfrac{1}{2}[1-(1-\eta)^{1/2}]\} -2(1-\eta)^{1/2}E\{\tfrac{1}{2}[1-(1-\eta)^{1/2}]\})/3\eta K(\eta)\,, \tag{59}$$

$$\sigma(\eta,\tfrac{1}{2}b)=2^{1/2}\pi[1-E(\eta)/K(\eta)]\,, \tag{60}$$

$$\sigma(\eta,b)=2^{3/2}(1-\eta)^{1/2}[K(\eta)-E(\eta)] \times[(1+\eta)E(\eta)/(1-\eta)K(\eta)-1]/3\eta\,, \tag{61}$$

$$\sigma(\eta,\tfrac{3}{2}b)=\sigma(\eta,\tfrac{1}{2}b)/(1-\eta)\,, \tag{62}$$

$$\sigma(\eta,2b)=2^{3/2}[K(\eta)-E(\eta)][(1+14\eta+\eta^2)E(\eta) -(1-\eta)(1+7\eta)K(\eta)]/15\eta(1-\eta)^{3/2}K(\eta). \tag{63}$$

The quantities described by Eqs. (58)–(63) are plotted in Fig. 9 as functions of the transverse oscillation frequency. For $c\leq\frac{1}{2}b$, $\sigma(\eta,c)<\frac{3}{2}$ and Eq. (56) may be re-

placed accurately enough by

$$\Delta\tau/\tau < (-dE/dz)_{E=E_0}/bV_0^{1/2}E_0^{1/2}. \quad (64)$$

Using the parameters listed in Table III, the maximum error in the period of oscillation is estimated to be about 0.5% for 60-MeV I ions and about 0.25% for 3-MeV He ions. The error is slightly larger for {111} channels than for {100} channels.

The error introduced into the model by neglect of the inelastic term in Eq. (8) is thus seen to be entirely tolerable. Even for particles making a substantial number of oscillations in passing through the crystal, the transverse motion is rather satisfactorily described by Eq. (29).

VIII. POPULATIONS OF SPECTRAL GROUPS

The model described in the foregoing sections gives an excellent quantitative account of the positions of the groups observed in the channeled-ion energy-loss spectra and of the way in which they depend upon the angle of incidence of the ion beam, the pathlength through the crystal, and the angular location of the detector. It is also necessary to consider the predictions of the model concerning the numbers of particles to be found in each of the several groups and the way in which these populations depend upon the experimental parameters. A brief discussion of this problem has been given previously by von Jan.[21] Since the initial impact points of the incident ions are uniformly distributed across the channel, Eqs. (11), (24), and (30) could be used to derive explicit formulas for the populations of various groups, ignoring beam divergence, crystal mosaic spread, and the influence of energy loss on the emergent angles. Even with these assumptions, the resulting expressions are exceedingly cumbersome, and removal of the restrictions complicates matters further. Therefore, the unrestricted model was made the basis of a computer program used to simulate some of the experiments described by Datz *et al.*[2] Monte Carlo methods were used as a matter of convenience to select the initial coordinate x_0 and the mosaic block misalignment angle. These angles were drawn from a Gaussian distribution about the mean crystal plane. It was assumed that each mosaic block ran entirely through the crystal. Since the divergence of the incident beam was less than the acceptance angle of the detector,[1] no allowance was made for beam divergence and the effects of multiple scattering were ignored. Having selected the initial conditions, Eq. (30) was used to find the emergent angles, and Eq. (40) was used for the final energy, with Eq. (52) for the stopping power. The resulting pair of events was scored on an appropriate histogram, and the calculation was repeated until a sufficient number of events had been accumulated. The program, run on an IBM System/360 Model 75 computer, required about 2 min to evaluate 10^5 events. The accompanying figures illustrate some typical results. In all cases but the last, the parameters of the calculation were those listed in Table III, chosen to simulate the experiments as closely as possible.

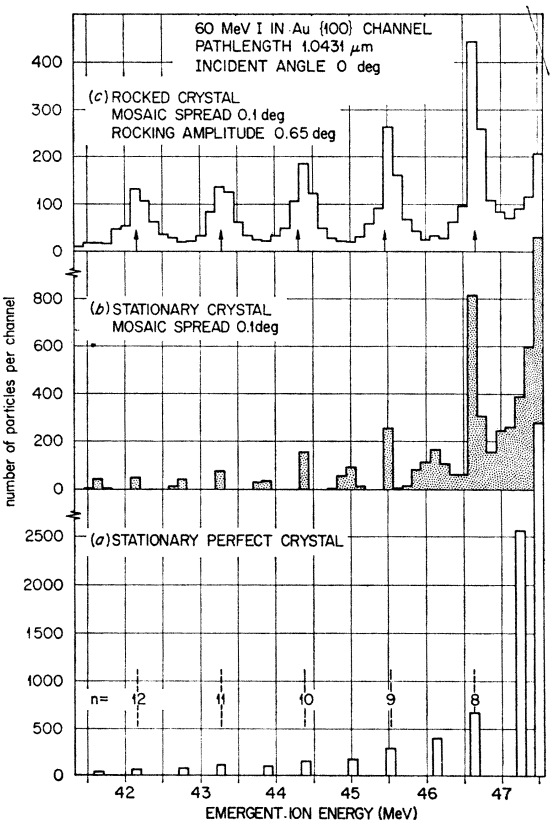

FIG. 11. Collinear energy-loss spectra computed for 60-MeV I ions incident upon Au {100} channels, showing the effects of crystal mosaic spread and of rocking the crystal. The arrows in panel (c) show the positions of the experimentally observed groups (Ref. 1). Model parameters are listed in Table III.

Figure 10 compares complete histograms calculated for perfect crystal targets with the ions incident parallel to the channel plane and slightly inclined to it. These histograms are analogous to Fig. 4 and may be interpreted analogously. It will be noted in the oblique incidence histogram that the points of highest intensity do not occur for a collinear detector, that is, at $\psi=\psi_0$, but for an emergent angle a little greater than the incident. This occurs because, when $\dot{x}$ (or ϑ) returns to its initial value after some integral number of periods, $\dot{z}$ has decreased due to the stopping power of the medium, thus increasing the emergent angle [see Fig. 1 and Eq. (26)]. Nevertheless, the groups are observed at essentially the same energies in both histograms, as expected from a consideration of Eq. (30). The slight deviations from this rule are probably connected with the "graininess" of the histogram.

The effects of crystal misalignment on the energy-loss spectra computed for a collinear detector are illustrated

[21] R. von Jan, Phys. Rev. Letters 18, 303 (1967).

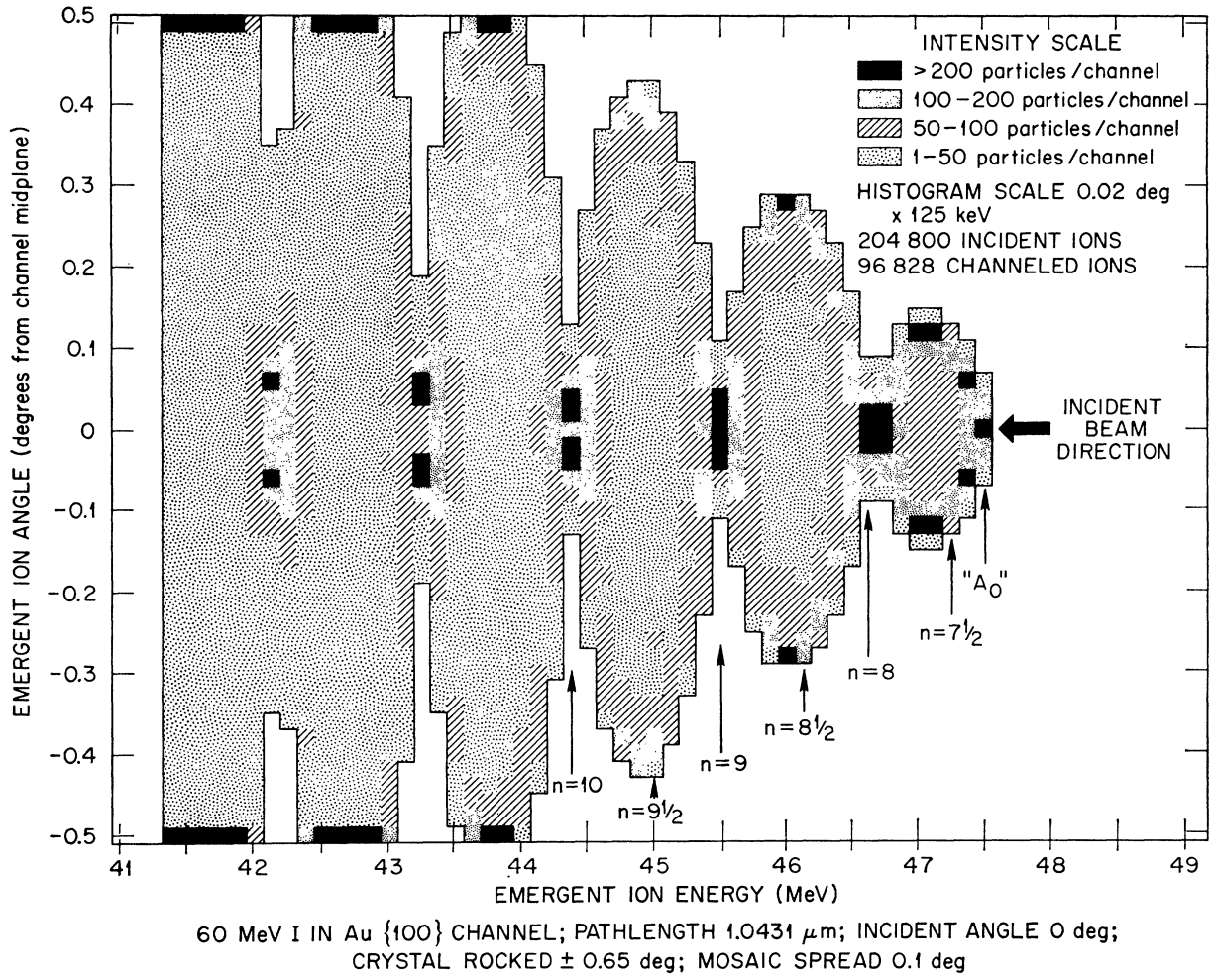

FIG. 12. Complete energy-loss spectrum computed for 60-MeV I ions incident upon a rocked Au {100} channel. The high intensities at large angles and low energies are artifacts, resulting from the finite size of the histogram. Model parameters are listed in Table III.

in Fig. 11. The spectrum for the stationary perfect crystal [panel (a)] is taken from the histogram of Fig. 10. Both integer and half-integer groups appear and the leading group A_0 is particularly intense. When a small Gaussian mosaic spread is introduced [panel (b)], all groups persist, but the half-integer groups are reduced in height and broadened, making the integer groups stand out more prominently in the spectrum. The mosaic spread assumed in the calculation is smaller than that found in most of the experimental targets. Finally, when the crystal is rocked through a large amplitude, the spectrum of panel (c) is found. The rocking amplitude (0.65°) exceeds the critical channeling angle (~0.5°) and completely overshadows the mosaic spread. The half-integer groups are now reduced to the level of background and the integer groups rise from rather broad bases. The A_0 group is strongly reduced in intensity, and the populations of the low-energy groups are greatly enhanced. As a result, the spectrum obtained by rocking the crystal is significantly cleaner and easier to interpret. The comparison between the model and the experiments is shown by the arrows in panel (c). Many of the experimental results reported by Datz *et al.*[1] were obtained by the rocking method, so that the usefulness of the technique is firmly established. The complete histogram computed for a rocked crystal is shown in Fig. 12. The close similarity of this histogram to those in Fig. 10 is evident. However, the nodes occur only for integer groups, the half-integer groups corresponding approximately (but not exactly) to the antinodes. Emergent ion angular distributions are shown in Fig. 13 for several final energy values. The clearly different angular distributions for integer and half-integer groups make the former quite easy to distinguish.

A number of calculations were made of the intensity of the A_0 group as a function of crystal pathlength, with the results shown in Fig. 14. This group is observed at all pathlength values, whenever the beam is incident in the channel plane, because of the finite acceptance

angle of the detector. It has, generally, no connection with the integer nodes discussed previously. The curve obtained for the perfect crystal features a series of sharp maxima at roughly constant intervals. Although there is a slight damping of these peaks as the pathlength is increased, they persist beyond 1 μm. As Eq. (38) indicates, a group of particles corresponding to a given number of oscillation periods, either integer or half-integer, can occur only over a limited range of channel pathlengths. Each peak in the perfect-crystal curve of Fig. 14 corresponds to the limiting thickness above which a particular group is no longer possible. Near this thickness, the population of the group rises and its position in energy approaches that of the A_0 group. Finally, it becomes indistinguishable from A_0 and disappears. As indicated in the figure, the peaks may be labeled with the values of n which disappear at each. The corresponding thicknesses may be regarded as the appropriate multiples of the wavelengths of the oscillating ions, although because of energy loss successive wavelengths decrease slowly. Introduction of mosaic spread into the crystal suppresses the strong fluctuations in the intensity of A_0, as shown by the lower curve of Fig. 14. There is some remnant of the $n=1$ peak, but no other significant fluctuation is observed. With smaller degrees of mosaic misorientation, the integer peaks persisted to greater thicknesses, but the half-integer peaks were totally suppressed. In the experimental work,[1] no evidence was found for such intensity fluctuations, in general agreement with the calculations.

Finally, it is necessary to comment on the experimental observation[1,2] that the structure observed for $\vartheta_0 \neq 0$ is strikingly sharper than that for $\vartheta_0 = 0$, when the target crystal is stationary. In the original report,[2]

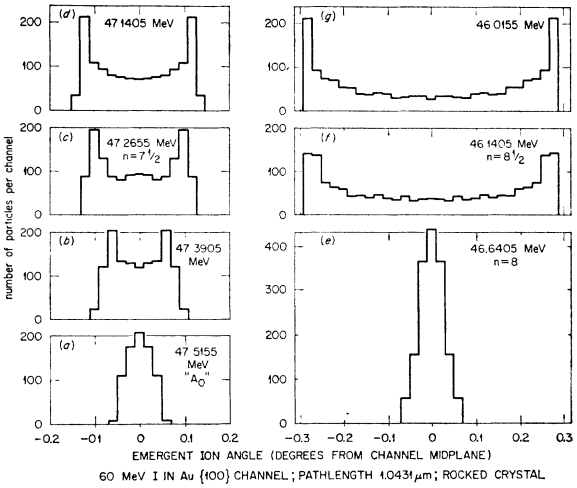

FIG. 13. Emergent angle spectra computed for several energy losses. These are cross plots of portions of Fig. 12.

this was attributed to the filling of the valleys between the integer groups by half-integer groups when $\vartheta_0 = 0$. The calculations generally support this interpretation. As Fig. 11 shows, the half-integer groups persist, though broadened, when small amounts of mosaic misorientation are introduced into the crystal. However, as the angle of incidence is changed from $\vartheta_0 = 0$, the half-integer groups move rapidly away from the collinear detector to the opposite side of the crystal plane. The phase-sensitive groups that replace them have lower populations, thus leading to more pronounced structure. That this is indeed the correct explanation is supported by the observation of much clearer structure when the target crystal is rocked through a substantial angle. The rocking amplitude simulates a very large

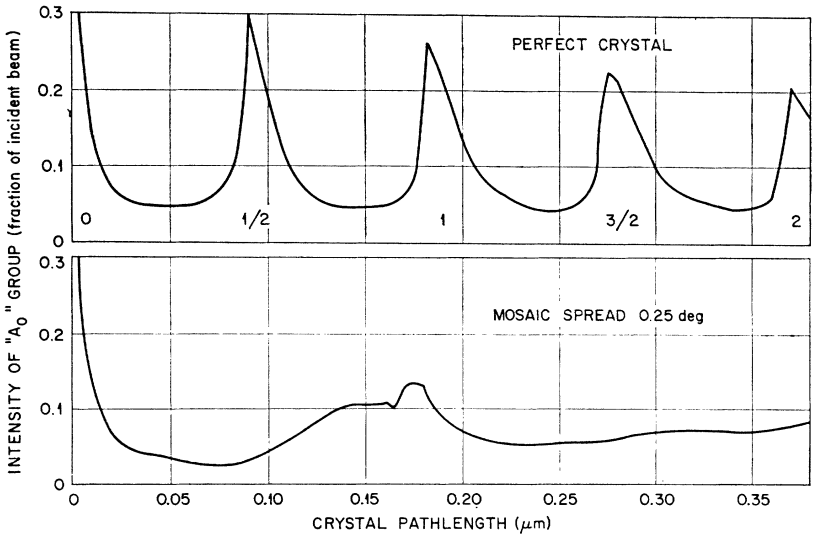

FIG. 14. The intensity of the A_0 group as a function of crystal pathlength, for 60-MeV I ions in Au {111} channels. The beam was incident in the channel plane. The model parameters were $Z_1Z_2 = 4187$, $b = 4.094$ Å^{-1}, $p = \frac{1}{2}$, $s_0E_0^{1/2} = 1078$ eV/Å, and $s_1E_0^{1/2} = 835.2$ eV/Å.

mosaic misorientation, with only the integer groups remaining significant features of the spectrum, as described above.

The width of the peaks observed in the energy-loss spectra depends upon a number of factors: the role of the target mosaic spread has been emphasized. The acceptance angle of the detector is also important, as may be seen from Figs. 4, 10, and 12. Thickness variations in the target influence the width of the peaks as well, since variations in ξ imply variations in the amplitude of oscillation corresponding to a given value of n. If ξ increases above the mean value, the amplitude of the particles reaching the detector must decrease and the stopping power which they experience must decrease as well. The decreased value of the stopping power is at least partially offset by the increased thickness, however. Datz *et al.*[1] have observed that ΔE for a given group is nearly independent of target pathlength for both I ions and He ions, suggesting that thickness variations play only a minor role in their experiments. The divergence of the incident beam is very important in determining the content of the observed spectrum, as may be seen from Figs. 4, 10, and 12. As was pointed out in Sec. IV, if the beam divergence is at all large, the structure of the spectra will be entirely eliminated. Each peak also has a width resulting from the statistical way in which the channeled ions encounter the electrons of the medium. Conventional theories of energy straggling presumably require alterations to allow for the crystalline structure of the medium before they can be applied to channeled-ion energy-low spectra. Additional multiple-scattering effects result from the nuclear interactions, because of the atomic nature of the crystal planes which is ignored by the model. This leads to broadening of the transmitted beam parallel to the crystal planes.

The items contributing to the width of the observed groups are partially under experimental control. It is perhaps well to emphasize again the importance of a small divergence in the incident beam and of a small acceptance angle in the detector, these being essential to the observation of well-resolved spectral groups. On the other hand, the mosaic misorientation of the crystal and small variations in its thickness are less important, and the former may, in fact, be of no particular significance if only experiments with a collinear detector are performed.

IX. CONCLUSION

The model described above gives a satisfactory account of the energy-loss spectra produced in beams of He and I ions transmitted through planar channels in thin Au monocrystals. The interatomic potential parameters derived from the data of Datz *et al.*[1] are in reasonable agreement with *a priori* expectations. Somewhat similar experiments[22] on 3- to 11-MeV protons transmitted through rather thick Si and Ge crystals failed to show any similar structure in the energy spectra observed from {111} and {110} channels. If the expected channeled-ion wavelengths are calculated for these cases using Eqs. (13), (14), (17), (24), (25), (31), and (34), they prove to be comparable to those for He and I ions in Au planar channels, ranging from 0.11 to 0.18 μm at 1 MeV, depending on the particular case. Two possible reasons for the lack of spectral structure may be suggested. First, the stopping power may depend less strongly on the coordinates than is the case for He and I ions in Au. This would make the expected groups more difficult to resolve. Second, the rather large thickness of the crystals may be responsible. At 8-μm pathlength and 5-MeV proton energy, the ions oscillate 20–25 times in Si {110} channels, for example. The resulting 40–50 approaches to the crystal planes should greatly increase the chances of an ion's being dechanneled, by thermal vibrations, crystal defects, or escape through the plane. Since the experiments of Datz *et al.*[1] suggest that He ions are more easily dechanneled in Au than are I ions, it is reasonable to expect even easier dechanneling of protons. It would be desirable to investigate these possibilities using much thinner crystals, but spectra as rich as those observed in Au cannot be expected. For example, 5-MeV protons will make only 2.8–4.2 oscillations in a 1 μm Ge {111} channel, so that only two or three peaks would be anticipated in the energy-loss spectra.

Although the original objective[2] of the direct determination of atomic-interaction potentials from energy-loss spectra has been frustrated by difficulties, principally the mosaic spread of the crystal, it has nevertheless been possible to account for several aspects of these spectra by assuming a reasonable form for the potential and deriving its plausible parameters from the data. More usefully, the data allow the determination of the coordinate dependence of the stopping power, about which little has been known previously. It remains for future investigations to examine the applicability of the function inferred to other energies, ions, and targets, and to establish a theoretical basis for it.

ACKNOWLEDGMENTS

It is a pleasure to express my sincere appreciation to B. R. Appleton, S. Datz, H. O. Lutz, C. D. Moak, and T. S. Noggle for many stimulating and fruitful discussions of the energy-loss spectra and their explanation of them, and for providing the experimental data used in the analysis. I am also grateful to D. K. Holmes and F. W. Young for many discussions and much encouragement during the course of this investigation.

[22] B. R. Appleton, C. Erginsoy, and W. M. Gibson, Phys. Rev. 161, 330 (1967); B. R. Appleton (private communication).

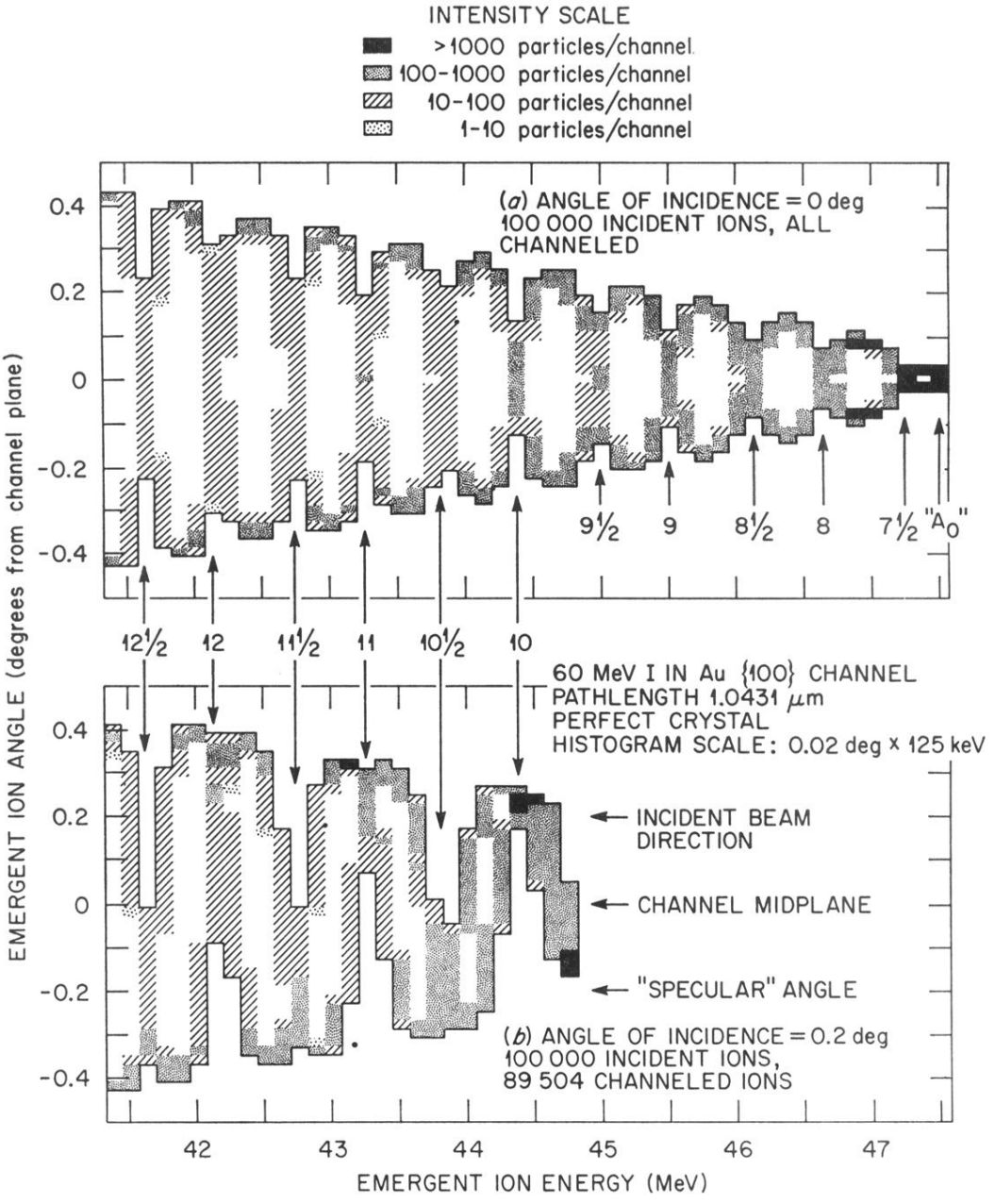

FIG. 10. Complete energy-loss spectra computed for 60-MeV I ions incident upon a perfect Au {100} channel, showing the effects of the incident angle. Model parameters are listed in Table III.

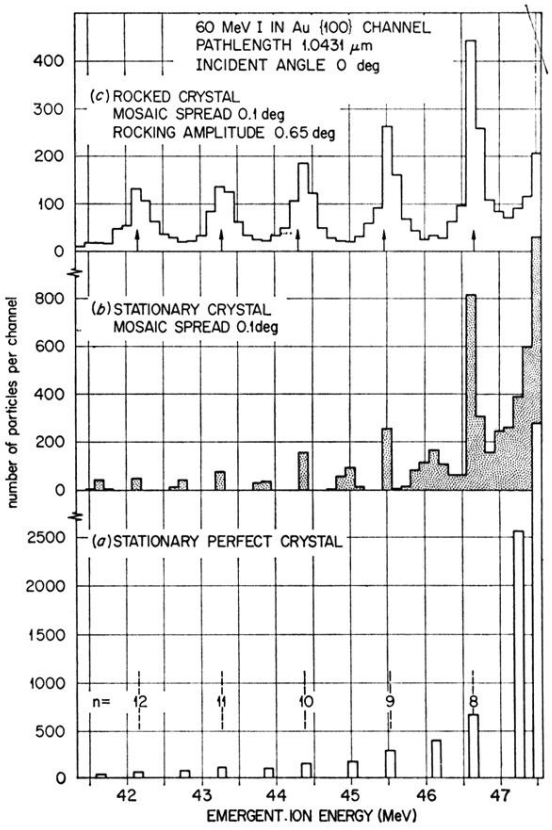

FIG. 11. Collinear energy-loss spectra computed for 60-MeV I ions incident upon Au {100} channels, showing the effects of crystal mosaic spread and of rocking the crystal. The arrows in panel (c) show the positions of the experimentally observed groups (Ref. 1). Model parameters are listed in Table III.

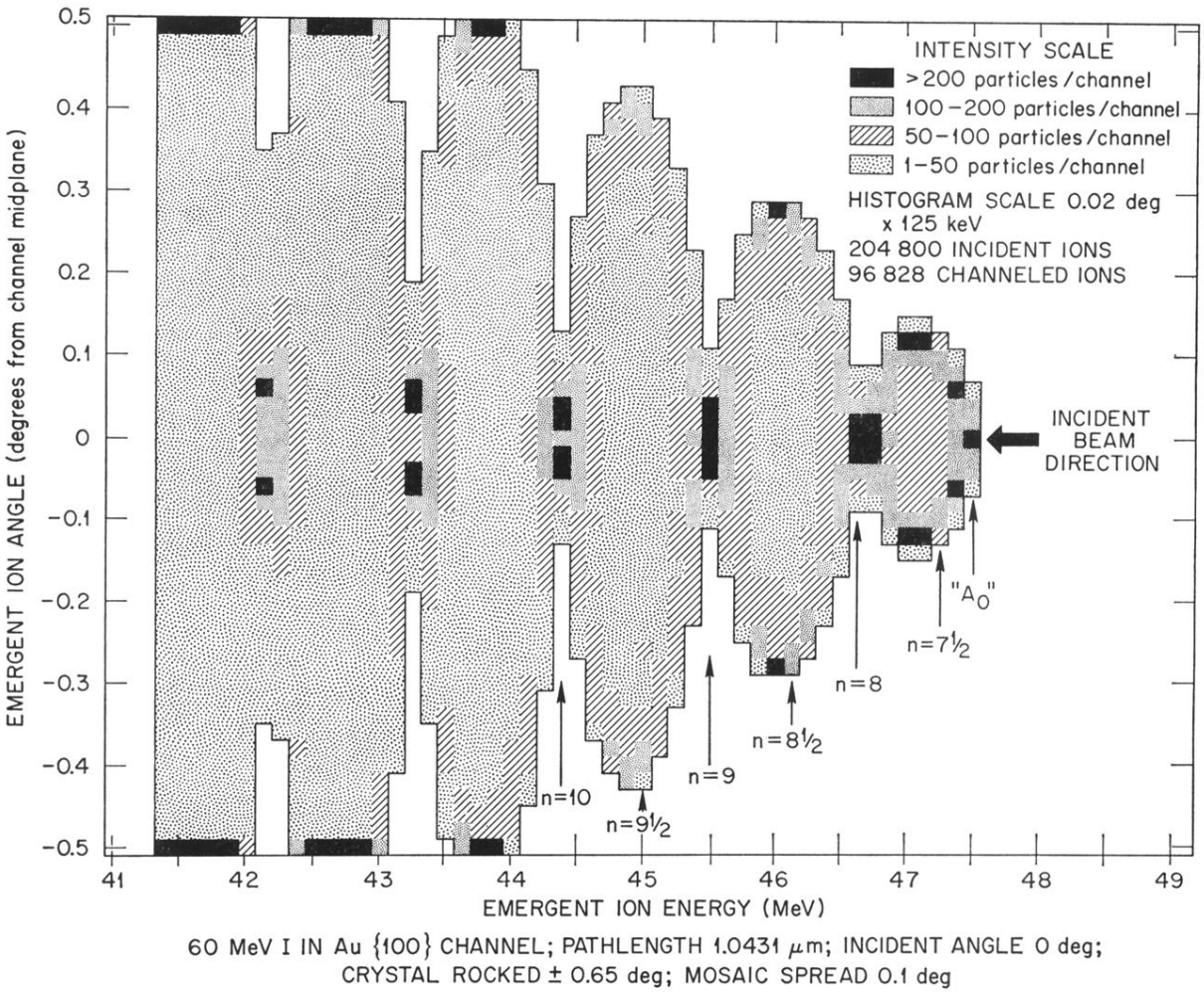

FIG. 12. Complete energy-loss spectrum computed for 60-MeV I ions incident upon a rocked Au {100} channel. The high intensities at large angles and low energies are artifacts, resulting from the finite size of the histogram. Model parameters are listed in Table III.